Composite Structures 271 (2021) 114168

Contents lists available at ScienceDirect

Composite Structures

journal homepage: www.elsevier.com/locate/compstruct

A dissection and enhancement technique for combined damage characterisation in composite laminates using laser-line scanning thermography

Haochen Liu [a], Weixiang Du [a], Hamed Yazdani Nezhad [b,*], Andrew Starr [a], Yifan Zhao [a,*]

[a] School of Aerospace, Transport and Manufacturing, Cranfield University, Cranfield MK43 0AL, UK
[b] Aeronautics and Aerospace Research Centre, Department of Mechanical Engineering & Aeronautics, City University of London, London EC1V 0HB, UK

ARTICLE INFO

Keywords:
Impact combined damage
Inter-laminar delamination
Laser scanning thermography
Damage quantitative dissection
Stationary wavelet enhancement

ABSTRACT

Impact induced combined damage in composite laminates attracts great attention due to its significant degradation of the structural integrity. However, the provision of the quantitative analysis of each damage portion is challenging due to its bare visibility and structural mixture complexity, so-called barely visible impact damage (BVID), which is referred to as inter-laminar delamination, and is inherently coupled with in-plane transverse and matrix damage also known as combined damage. Instead of focusing on one type of damage in most of the existing studies, this paper proposes a decomposition and targeted enhancement technique based on Stationary Wavelet Transform (SWT) for such coupled BVID in composite laminates using laser-line scanning thermography. Firstly, a combined damage model composed of in-plane damage and inter-laminar delamination is established by finite element numerical modelling to predict the thermal response pattern in the laser scanning thermography. Then, a feature separation and targeted enhancement strategy based on SWT in the frequency domain is proposed to improve the contrast of the matrix crack and delamination in combined damage scenarios induced by low-velocity rigid impact via drop-tower tests, meanwhile eliminating noise and suppressing the laser pattern background. The enhanced images of in-plane damage and delamination are furtherly processed by Random Sample Consensus (RANSAC) method and confidence map algorithms to calibrate the damage profile. The proposed technique is validated through inspecting a group of unidirectional carbon fibre-reinforced polymer composite samples, impacted by a variety of energy levels, in fibre-parallel (0°), 45° and orthogonal scanning modes. The results demonstrate that the proposed technique can pertinently isolate, enhance and characterise the inspected in-plane crack and inter-laminates delamination in a flexible manner. The proposed methodology paves the way towards automated infrared thermography data analysis for quantitative dissection of actual combined damage in composite laminates.

1. Introduction

Carbon fiber-reinforced polymer (CFRP) composite plays an increasingly dominant role in material science, technology innovation and advanced structures. Due to its advantages of low density, high structural strength, adjustable mechanical properties and high resistance to corrosion and abrasion, CFRP keeps attracting the attention and extending the structural applications in aerospace, space, automotive, nuclear, civil and renewable energy sectors [1,2]. With the demands for lighter weight and environmental sustainability and the increasing cost associated with fossil fuel consumption, modern aviation and transportation structures manufacturers are focused on CFRP, glass fibre-reinforced polymer (GFRP) and advanced composites and nanocomposites as alternatives for enhanced structural and chemical performance superior to metallic counterparts. In aviation, a new generation of airplanes emerges with a growing ratio of composite usage in key components known as primary structures, including radar radome, fuselage, wing panel, engines, etc. [3]. However, the component integrity and mechanical stability of advanced composites, e.g., composite laminates, is threatened by damage and degradation caused by low-velocity impact, maintenance tools or ground vehicle strikes, long period overloading and severe or varying service environment. Ostensibly, surface damage profiles such as those identified as barely visible impact damage (BVID) are relatively small, and seem to be

* Corresponding authors.
E-mail addresses: haochen.liu@cranfield.ac.uk (H. Liu), W.Du@cranfield.ac.uk (W. Du), hamed.yazdani@city.ac.uk (H. Yazdani Nezhad), a.starr@cranfield.ac.uk (A. Starr), yifan.zhao@cranfield.ac.uk (Y. Zhao).

https://doi.org/10.1016/j.compstruct.2021.114168
Received 21 February 2021; Revised 12 May 2021; Accepted 21 May 2021
Available online 24 May 2021

harmless, i.e. falling within the allowed damage size according to the aircraft's structural repair manual. But internal structural damage could be fatal and penetrating through the material may result in catastrophic failure [4].

It has been observed that the structural integrity in aerospace-grade composite laminates or composite-composite bonded joints is substantially reduced by more than 50% dissipation of strain energy (key parameter to the load-carrying capacity of a composite structure), mainly due to inter-laminar delamination, polymer matrix debonding [5,6] and matrix cracking [7]. Such combination of inter-laminar delamination and in-plane damage, so-called combined damage [8], may be further followed by fibre bundle breakage or severe re-orientation at increased strain energy, e.g. due to further mechanical loading that ultimately leads to the structural rupture (i.e. ultimate failure). Such ultimate failure is instantaneous and along with a dramatic reduction in the structural integrity and must be avoided. Therefore, reliable health monitoring and non-destructive inspections are required to measure the combined damage and its progression occurring prior to fibre bundle breakage.

Among such pre-mature damage types in CFRP, matrix cracking and inter-laminar delamination are two typical types of damage caused by relatively high-energy and low-velocity impact, and have the prevailing influence on the performance of CFRP, i.e. the impact energy dissipated by damage mechanisms is much higher than those reversible ones induced by deformation mechanisms (e.g. elasticity) [9]. Delamination caused by high inter-laminar stresses could weaken strength to carry loads through thickness strength [10]. Simultaneously, due to the structural characteristics of multiple layers containing different fibres orientations, impact damage often leads to combined damage presenting as individual fibres and transverse matrix cracks overlapping with delamination [11–13]. It is essential and valuable to quantitatively assess penetration damage in diverse impact energy for material life-cycle assessment and structural maintenance. However, it is difficult to directly estimate the through-the-thickness damage from the impact side as severe surface damage affects and outweighs the inspection result of the subsurface damage. Therefore, it is pivotal to non-destructively inspect and distinguish those hidden and less visible combined damage with cracks and delamination overlapped.

Infrared thermography (IRT) is a powerful NDT technique that offers rapid, non-contact, robust non-invasive inspection and real-time monitoring. With many practical applications for ceramics, plastics and composites [14–16], it has presented advantages in material suitability, inspection efficiency and cost budget compared to other NDT technique such as eddy current testing, ultrasonic, radiographic inspection in many specific scenarios [17–20]. Among the diverse external sources of active thermography, the laser is a promising source for the inspection of small-scale damage in complex structured composites. Due to the advantages of high energy concentration, heat density, precise directionality and multifarious shapes of heating pattern, the laser provides a more suitable alternative than the traditional lamp and contact heating for small local defects [16], such as surface crack and subsurface delamination in composite material. For the inspection of delamination only, Ultrasonic inspection can achieve better detection depth but is limited due to blind surface detection issue and contacting necessity. Compared to radiography, the proposed method has the advantage of inspection speed and low cost but it may not be able to build the whole defect profile as 3D Tomography. Compared to electromagnetic testing like eddy current inspection, it may not be that sensitive to tiny cracks but will stand out at delamination detection. By aiming on combined damage breakdown in composites, this research focus on the inspection solution to distinguish between different damage mechanisms, and achieve a good balance for seperately crack and delamination inspection at the same time, especially for the combined defect scenario in impact damage.

A line or a spot of a laser beam is the basic heating unit to provide highly stable heat penetration along the expansion surface and through the thickness [21]. Furthermore, moving spot and line has been applied to solve the shortcoming of the low efficiency in inspecting large metallic and composite structure [22,23]. Then the laser heat patterns were improved with Laser Array Spot Thermography (LAST) which also provides clear thermal contrast of defect edge [24,25]. Compared to a laser array pattern, the line-laser heating is easier to be manipulated and calibrated, more homogenous along the line and with lower costs. But its thermal contrast of inspection results is more dependent on the crack direction. On the other hand, both spot, line pattern and array pattern have been applied in the inspection of subsurface delamination and wall-thinning in composite laminates [26,27]. However, by only focusing on one type of defect (wall-thinning, crack or delamination) properties, these researches are not applicable to the analysis of the impact damage portion individually. The thermal behaviour and characteristic features of impact damage in thermography are composed of diverse thermal image properties throughout the image sequence. Due to the interacting influence of thermal image properties in both time and frequency domains caused by overlayed damage types (matrix crack and delamination), the conventional thermal image processing methods for single defect type are not suitable for further accurate defect quantification analysis [28,29]. Therefore, it would be reasonable to investigate an applicable defect feature dissection method to characterise and distinguish the matrix cracking and delamination for enhanced damage analysis for reliable life assessment and maintenance. To address the challenge of the combined damage mentioned in Fig. 1, a damage decomposition and enhancement technique is proposed to pertinently preserve crack and delamination, and to coordinate noise-cancelling and heat background suppression for the combined damage inspection using Laser-Line Scanning Thermography (LLST) (Fig. 1).

In the current article, the development of a novel image processing technique based on Stationary Wavelet Transform (SWT) for combined damage identification and dissection in composite laminates based on LLST is presented. The development of finite element modelling (FEM) is presented in Section 2 to study thermal characteristics of LLST for combined damage texture and geometry. A technique for defect properties decomposition and enhancement is proposed in Section 3 to pertinently characterise the crack and delamination overlapped in combined damage, respectively. Experimental setup and associated results are then presented to validate the proposed method in Section 4, and the conclusions are provided in Section 5.

2. FEM simulation

In order to comprehensively investigate thermal features and conduction characters in the LLST inspection for different types of defects in CFRP, a numerical simulation based on FEM has been conducted as

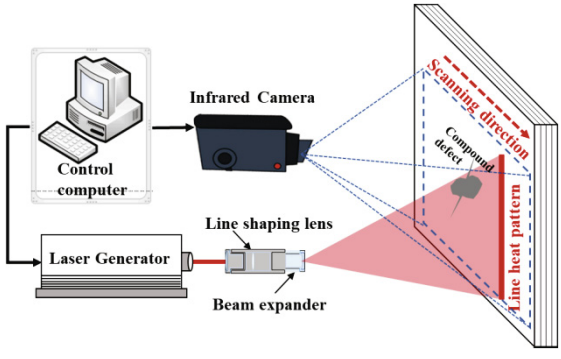

Fig. 1. Principal of Laser-line scanning thermography system.

a convenient approach for the provision of flexibility and stability for signal prediction. Fig. 2 presents the basic principle of LLST for CFRP inspection. The steps are as follows:

1. A continuous-wave line-shaped laser is conducted to heat the object surface in one direction scanning manner.
2. The spatially dynamic heat flux absorbed by the sample will create a thermal front that transfers inside the material and perturbs the heat diffusion flow when it reaches defects or internal discontinuity.
3. The combined damage composed of cracks and delamination interacts with the dynamic heat flow, and generates heat resistance in relation to their defect profiles, which eventually produces different but overlayed defect patterns during the scanning process.
4. Due to the overlapped feature of the defect, the 3D modelling of local crack and delamination in combined damage within composite layers is crucial to the signal prediction and defect feature analysis. In this research, the FEM is applied to establish the 3D combined defective model and dynamic thermal inspection process. The deployment of this modelling approach is realised in a transient regime, which thereby provides rapid and straightforward thermal data acquisition.

To derive a mathematical model from describing the heat transfer in CFRP material using the FEM [30], the following assumptions are considered:

1) The applied heat flux (scanning laser) is initially applied on the surface and unidirectional transferring in the Z-direction (Fig. 2);
2) The penetration of optical radiation through the material and thermal expansion are neglected;
3) The fibres are homogeneously distributed within the matrix and are uniform in shape and size;
4) The thermophysical properties of the material remain constant and are independent of temperature;

As depicted in Fig. 2, the CFRP composite laminate is comprised of multiple plies of CFRPs with a consistent thickness [31]. Based on the Fourier heat transfer law, the governing equation of thermal conduction in anisotropic material is given by [32]:

$$[\kappa]_{An}\{\nabla\}^T\{\nabla\}T - (\rho c_p)_{eff}\dot{T} = -\mathrm{Q}|_{\Gamma(\mathrm{X(t)},\mathrm{Y(t)},\mathrm{t})} \tag{1}$$

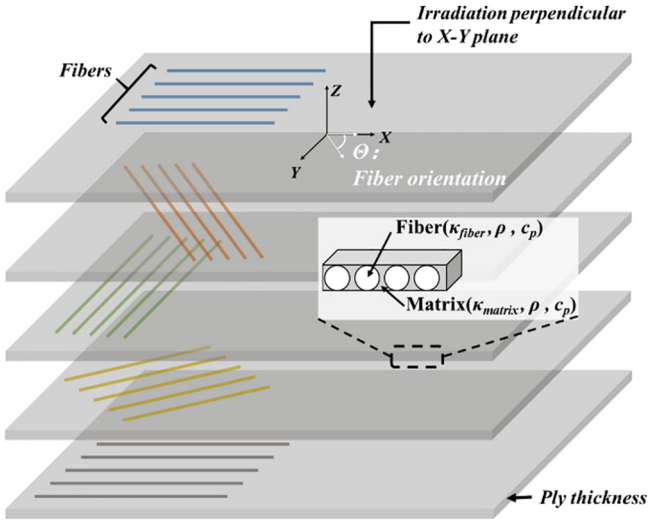

Fig. 2. Modelling structure of CFRP.

where T and $\{\nabla\}$ denote the temperature and gradient vectors along with the Cartesian coordinates. $[\kappa]_{An}$ and $(\rho c_p)_{eff}$ denote the global anisotropy of heat conductivity and effective volumetric heat capacity of the material, respectively. As for the boundary condition accounting for external scanning heat, the $-\mathrm{Q}|_{\Gamma(\mathrm{X(t)},\mathrm{Y(t)},\mathrm{t})}$ is the scanning excitation heat flux, in which $\Gamma(\mathrm{X(t)},\mathrm{Y(t)},\mathrm{t})$ determines the spatially dynamic heat area on the surface. The dynamic heat flux moving along the XY plane is determined by the width and length of the line beam and the scanning manner.

To account for the anisotropic composites, the thermophysical properties of the CFRP, which decisively control the modelling are discussed below. Via representing the matrix with epoxy-resin and reinforcements by fibres acting such as pores in the heat transfer model, the model is established as a porous structure. Based on the above description, the effective volumetric heat capacity given in Eq. (1) can be estimated based on volume fractions:

$$(\rho c_p)_{eff} = \phi_f(\rho c_p)_f + (1-\phi_f)(\rho c_p)_m \tag{2}$$

$$\phi_f = \frac{V_f}{V_T} = \frac{V_f}{V_f + V_m} \tag{3}$$

where ϕ_f denotes the volume fractions of the fibre. The subscripts f and m in Eqs. (2) and (3) denote the fibre and matrix, respectively.

To account for thermal conductivity, the series–parallel model [33] is employed. The longitudinal and transverse equivalent thermal conductivity -κ_L and κ_T corresponding to the X and Y directions (i.e. longitudinal and transverse directions) are given by:

$$\kappa_L = \kappa_f\phi_f + \kappa_m(1-\phi_f) \tag{4}$$

$$\kappa_T = \frac{\kappa_f\kappa_m}{\kappa_m\phi_f + (1-\phi_f)\kappa_f} \tag{5}$$

where κ_f and κ_m are the conductivity of fibre and matrix, respectively. After working out the κ_L and κ_T, the global heat conductivity can be calculated by:

$$[\kappa]_{An} = \begin{bmatrix} \kappa_L cos^2\theta + \kappa_T sin^2\theta & \frac{\kappa_L-\kappa_T}{2} sin2\theta & 0 \\ \frac{\kappa_L-\kappa_T}{2} sin2\theta & \kappa_L sin^2\theta + \kappa_T cos^2\theta & 0 \\ 0 & 0 & \kappa_{cp} \end{bmatrix} \tag{6}$$

where θ is the fibre orientation angle related to X-direction and $\kappa_{cp} = \kappa_T$ is the cross-ply conductivity. After establishing the objective model and discretisation using the Galerkin FEM and meshing using hexahedron element, the heat transfer with the model can be expressed by (7).

$$[\mathrm{K}]_{An}\{\mathrm{T}\} + [\mathrm{C}]\{\dot{\mathrm{T}}\} = \{\mathrm{Q}\}_{\mathrm{scan}} \tag{7}$$

$$\left[[\mathrm{K}]_{An}(1-\zeta) + \frac{[\mathrm{C}]}{\Delta\mathrm{t}}\right]\{\mathrm{T}\}_{\mathrm{t}+\Delta\mathrm{t}} = \{\mathrm{Q}\}_{(\mathrm{X}+\Delta\mathrm{X_t},\mathrm{Y}+\Delta\mathrm{Y_t},\mathrm{t}+\Delta\mathrm{t})} + \left[\frac{[\mathrm{C}]}{\Delta\mathrm{t}} - \zeta[\mathrm{K}]_{An}\right]\{\mathrm{T}\}_{\mathrm{t}} \tag{8}$$

where $[\mathrm{K}]_{An}$, $[\mathrm{C}]$ and $\{\mathrm{Q}\}_{\mathrm{scan}}$ stand for coefficient stiffness matrix of conductivity (e.g. $[\kappa]_{An}$), effective volumetric heat capacity (e.g. $(\rho c_p)_{eff}$) and dynamic heat flux, respectively. By using the time-domain integration solver, the temperature response can be simulated by (8), where $\zeta = 0.3$ is a convergence parameter.

Fig. 3 presents the FEM model of CFRP with a typical combined damage composed of horizontally laid delamination and a vertical crack in Y-direction representative of transverse matrix crack. A ten-layers of fibre ply model with a 45-degree angle difference of fibre orientation is established. The dimension of the CFRP model is 20 mm × 20 mm × 2 mm and the thickness of each layer (ply) is 0.2 mm. The model is discretised as 400 × 400 × 40 hexahedral elements. The laser-line is a Gaussian beam distribution (1/e fall) with

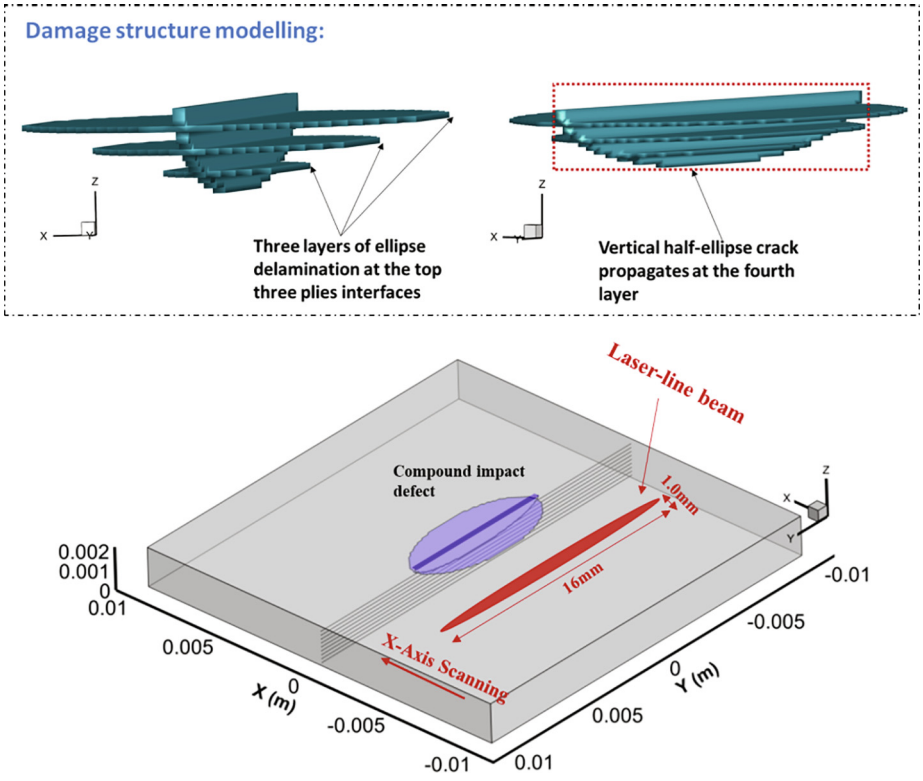

Fig. 3. The FEM modelling of CFRP with existing combined damage.

the size of [16 mm, 1 mm] for [length, width] axis. The dynamic beam scans along the X-direction with a speed of 10 mm/s.

As the impact energy penetrates through the multiple plies causing diverse and progressive inter-laminar delamination and matrix damage occurring between plies, the combined damage will be presented by mixed cracks and delamination through and along with fibre orientation. To focus on the main defect properties, the combined defect is simplified into two portions: vertically semi-circular crack and stacked multi-layered elliptic shaped delamination [7]. The damage is composed of three horizontal (XY planar) ellipse-shape delaminations at the top three plies interfaces and one vertical (YZ planar) half-ellipse crack propagating through the top fourth ply. The direction of the crack is modelled the same as the top ply's fibre direction. The crack width and delamination thickness are modelled to be 50 μm, representing the extent of damage reaching 25% of the ply thickness. The major and minor axes of half-ellipse crack are [8.0 mm, 1.6 mm]. Three ellipse delaminations are buried at the top three interfaces with the decreasing size layer-by-layer. The major and minor axes of three ellipse delamination are [8.0 mm, 3.2 mm], [6.5 mm, 2.4 mm] and [5.0 mm, 1.2 mm].

3. Image enhancement for defect visualisation

The main hypothesis of image enhancement in this study is that different types of defect, sound regions and noise have different frequency responses in the wavelet domain. By further manipulating the wavelet coefficients, defects can be enhanced and decomposed. The methodology, illustrated in Fig. 4, is mainly composed of: SWT-based defect feature decomposition and enhancement, enhanced feature image cumulation and defect visualisation. It can not only eliminate noise and suppress the influence of the laser background but also separately enhance and visualise crack and delamination which was the purpose for distinguishing in-plane damage from the delamination.

3.1. Stationary wavelet transformation (SWT)

In this research, the 2D stationary wavelet transform (SWT) is employed not only for denoising but also for decomposing different types of defects in combined damage. In SWT, the á-trous [34] algorithm principle and decomposition equation utilised in our research, given by

$$\begin{cases} A_{k-1}(m,n) = \sum_{i=1}^{M}\sum_{j=1}^{N} h^1_{l-m} h^2_{j-n} A_k(i,j) \\ D^1_{k-1}(m,n) = \sum_{i=1}^{M}\sum_{j=1}^{N} h^1_{l-m} g^2_{j-n} A_k(i,j) \\ D^2_{k-1}(m,n) = \sum_{i=1}^{M}\sum_{j=1}^{N} g^1_{l-m} h^2_{j-n} A_k(i,j) \\ D^3_{k-1}(m,n) = \sum_{i=1}^{M}\sum_{j=1}^{N} g^1_{l-m} g^2_{j-n} A_k(i,j) \end{cases} \tag{9}$$

where $A_{k-1}(m,n)$denotes the approximation coefficient at $k-1$scale. $D^1_{k-1}(m,n)$, $D^2_{k-1}(m,n)$and $D^3_{k-1}(m,n)$ denote the horizontal, vertical and diagonal wavelet coefficients, respectively. In Eq. (9), h^1_m, g^1_m, $h^2_n and g^2_n$ are the filters of wavelet decomposition transform which are related to the wavelet basis. (m,n) denotes the pixel coordinate within a $M \times N$ size image.

Compared to the traditional Discrete Wavelet Transform (DWT), the SWT poses advantages in several aspects which are suitable for the LLST inspection of combined damage scenario [35]:

1) As the SWT employs up-sampling wavelet filters, more details can be preserved in approximation, horizontal, vertical and diagonal coefficients after transformation. The combined damage features, especially for tiny cracks, are more possibly detected.
2) In SWT, the amplitude scale of approximation and wavelet coefficients after decomposition is larger (about twice) than the one before decomposition. The wide amplitude scale provides sufficient space for the threshold identification of the targeted feature in nonlinear transformation enhancement.

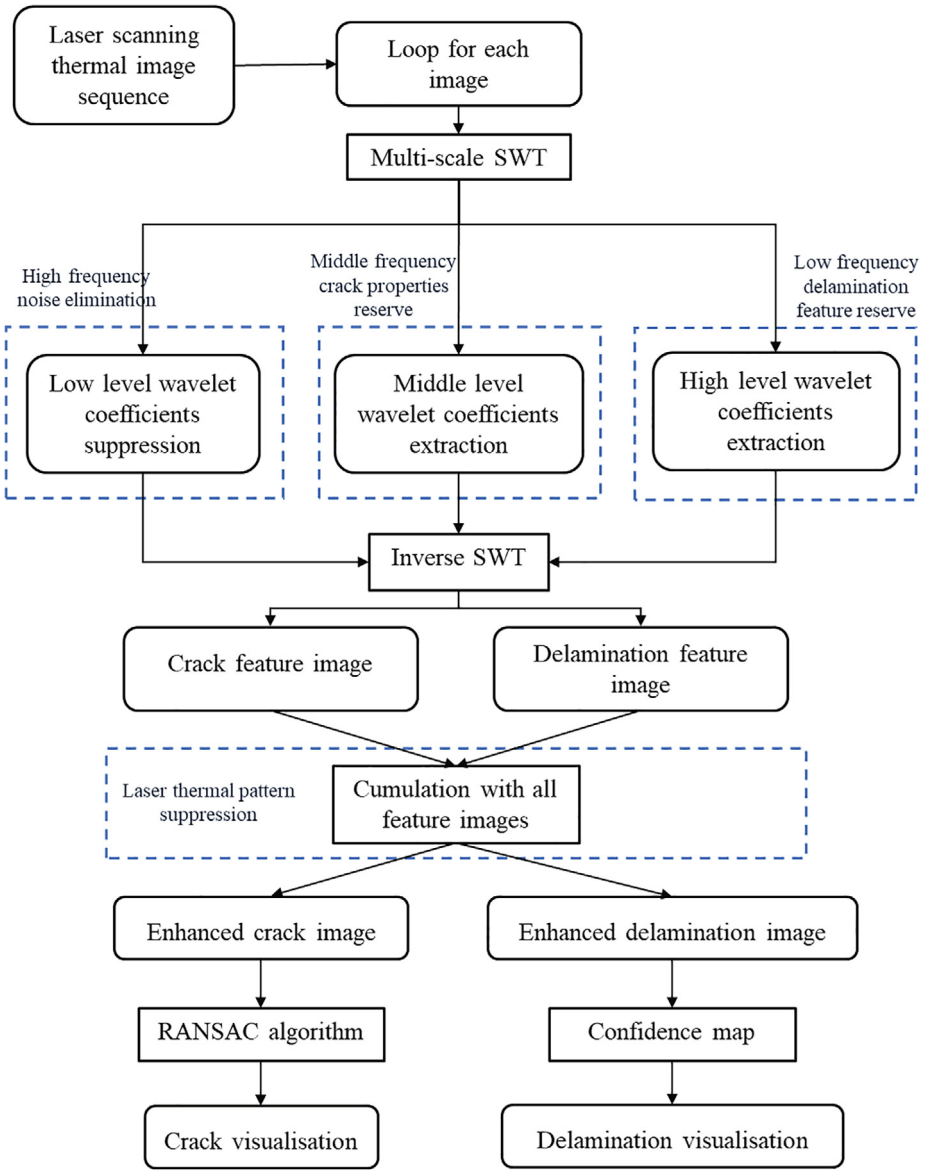

Fig. 4. Combined damage detection and visualisation methodology.

The approximation and the wavelet coefficients after SWT present the features of images properties in horizontal, vertical and diagonal directions (utilised herein), and also indicate different information in the frequency domain from the initial to final decomposition levels.

After the SWT decomposition, different defect feature will be captured at a different level of wavelet coefficient according to its wavelet frequency properties. By preserving the relevant coefficients and compressing the unneeded properties, the targeted defect feature can be individually extracted and enhanced by an inverse SWT reconstruction. Equation (10) denotes the calculation of the inverse SWT reconstruction.

$$A_k(m,n) = \sum_{i=1}^{M}\sum_{j=1}^{N} h^1_{l-m}h^2_{j-n}A_{k-1}(i,j) + \sum_{i=1}^{M}\sum_{j=1}^{N} h^1_{l-m}g^2_{j-n}D^1_{k-1}(i,j) + \sum_{i=1}^{M} \times \sum_{j=1}^{N} g^1_{l-m}h^2_{j-n}D^2_{k-1}(i,j) + \sum_{i=1}^{M}\sum_{j=1}^{N} g^1_{l-m}g^2_{j-n}D^3_{k-1}(i,j) \quad (10)$$

where, h^1_m, g^1_m, h^2_n, g^2_n are the wavelet reconstruction filters and are related to the wavelet basis; $A_k(m,n)$ is the inverse reconstructed enhanced image and $A_{k-1}(m,n)$ is the approximation coefficient at the $k-1$ level. $D^1_{k-1}(m,n)$, $D^2_{k-1}(m,n)$, $D^3_{k-1}(m,n)$ denote the modified or selected detail coefficients according to the enhancement demand and the image properties to be preserved.

3.2. Image processing procedure

The dynamic laser-line scanning along the CFRP impact combined damage generates a series of thermal images with complex signal properties in both spatial and time domain. Each thermal image, $I(m,n)$, contains the combined damage signals including the delamination $D(m,n)$ and the crack $C(m,n)$, the laser pattern background $B(m,n)$, the noise signal $N(m,n)$. The image $I(m,n)$is given by Eq. (11)

$$I(m,n) = D(m,n) + C(m,n) + B(m,n) + N(m,n) \quad (11)$$

Here, the properties of these signals are analysed as follows:

(1) Most of the noise signal N(m,n) is in high-frequency sub-bands in the frequency domain, which should be compressed for defect enhancement. It can be eliminated by using a low-pass filter in the wavelet domain.

Table 1
Enhancement strategy for different wavelet frequency property feature.

Information type	Information properties	Processing requirements	Processing methods
The noise signal N(m,n)	High sub-bands	Eliminating	SWT, Low-pass filtering
The delamination D(m,n)	Low sub-bands	Preserving and enhancing	SWT, Low sub-band preservation
The crack C (m,n)	Middle sub-bands with directionality	Preserving and enhancing	SWT, Middle sub-band preservation
The laser background B (m,n)	Middle sub-bands, spatial scanning	Suppressing	Enhanced Image sequence cumulation

(2) The defect signals: delamination $D(m,n)$ and crack $C(m,n)$ contain higher contrast than the background signal $B(m,n)$ and the noise $N(m,n)$. And both $D(m,n)$ and $C(m,n)$ are in lower sub-bands in the wavelet domain. Compared to $D(m,n)$, the crack $C(m,n)$appears sharply in the middle-frequency sub-band with strong spatial direction consistency simultaneously. $D(m,n)$ is in the low-frequency sub-band with strong regional connectivity. Both these signals should be preserved and can be separately enhanced with the preservation of specific sub-bands.
(3) The laser pattern background $B(m,n)$ depends on the line beam pattern, the location of which is changing by time. It is a distraction for defect visualisation and should be suppressed. It should be noticed that the narrow laser-line may sit in the middle-frequency sub-band in the wavelet domain and it is difficult to distinguish it from the crack $C(m,n)$. But its spatial position is changing compared to the still defects in the image sequence. Therefore, the cumulation of a sequence of images will effectively suppress the dynamic laser pattern and improve the contrast of still defects.

The frequency distribution of the image information, corresponding processing requirements and processing methods are summarised in Table 1.

3.3. Crack and delamination enhancement

To further extract the property of crack, the Random Sample Consensus (RANSAC) algorithm is employed to estimate parameters of a mathematical model of crack outliers. It is a non-deterministic algorithm producing reasonable results only with a certain probability by iterative calculations. It has been widely applied to geometric primitive detection, wide baseline matching, motion segmentation, robust feature image matching and other fields [36]. The extraction of the directional cracks is a typical line fitting processing problem in a two-dimensional point cloud dataset. It is essentially composed of three iterative steps:

1) Take a random subset of original data as hypothetical inliers.
2) A model is fitted to the set of hypothetical inliers. All other data are then tested against the fitted model. Those points that well fit the estimated model, according to a model-specific loss function, are considered as part of the consensus set.
3) Repeat the first 2 steps until the estimated model is reasonably good if satisfactory points have been classified as the consensus set. Otherwise, go to step 1 to improve the model using all members in the consensus set.

For the delamination visualisation, the enhanced image is then processed by a confidence map algorithm [37]. The confidence map transfers the intensity of thermal images into the confidence level of the inspection, which can highlight the true damage from the neighbouring regions.

4. Result and discussion

4.1. SWT simulation results

In this section, the simulated thermal response of the model shown in Fig. 4 is analysed. Fig. 5 presents the temperature distribution at 4 different time (0.15 s interval between each step) when the laser-line scans across the defect area. The thermal images of the top surface show an obvious temperature contrast on the delamination area and a dramatic discontinuity at the crack edge. It demonstrates that, when the laser is on the left side of the crack, the heat transfer is blocked by the crack and the right part is almost invisible. When the laser moves to the right side of the crack, the right part can be clearly observed but the left part of the delamination exhibits a dramatically reducing signal amplitude due to the heat diffusion and crack block effect. The difference of thermal pattern between delamination and crack indicates that it is wise to separately extract the features of each type of defect in the frequency domain rather than in the amplitude domain. Furtherly, the difference of transient thermal contrast in the scanning sequence not only confirms the above view but also suggests that it is essential to consider the image sequence of laser scanning across the whole combined damage.

Then, the proposed method is applied to the simulation image sequence to enhance and identify the crack and delamination. Fig. 6 presents crack and delamination identification results using the employed RANSAC and confidence map. It can be observed that the simulated crack and delamination profile is effectively marked. The

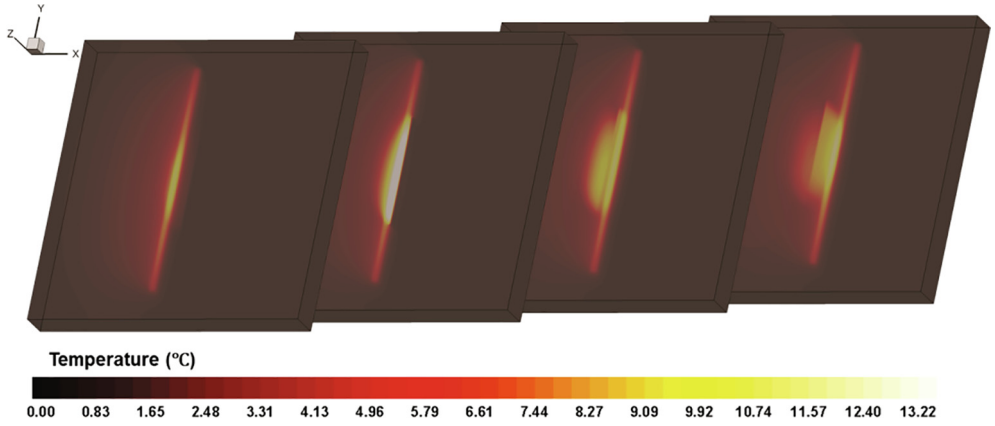

Fig. 5. The simulation results of laser scanning through the combined defect area.

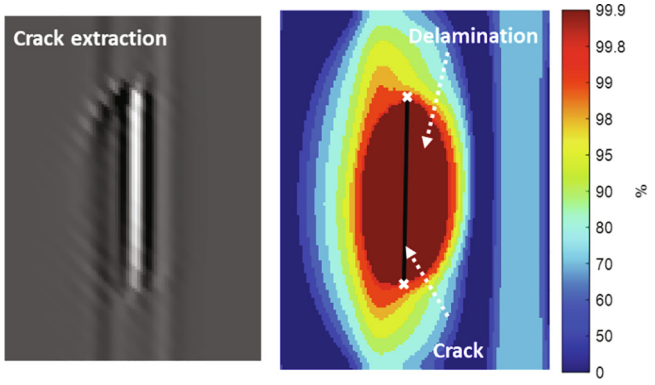

Fig. 6. The crack and delamination results on simulation data using the proposed method.

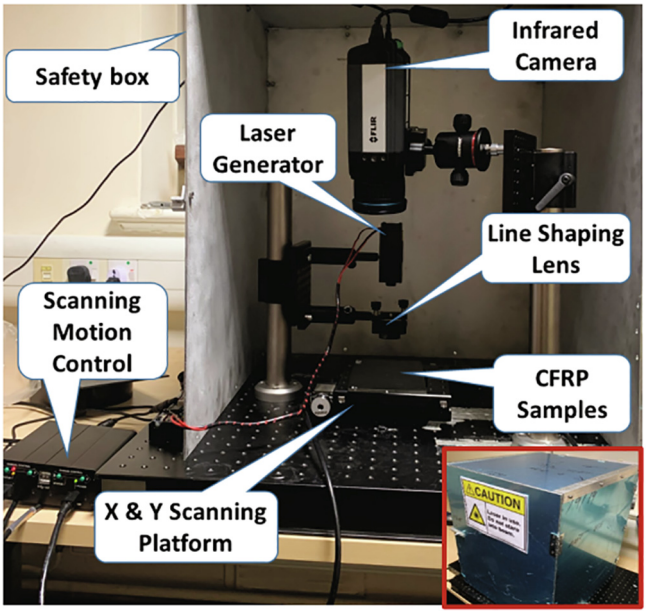

Fig. 7. Laser-line scanning thermography experimental system.

Table 2
Experiments specification parameters.

Items	Specification parameters
IR Camera	• IR wavelength range: 7–14 μm; • Thermal sensitivity: less than 25 mK; • Detector resolution: 640 × 512;
Laser-line heating source	• Continuous wave (CW) Bluary laser, 450 nm; • Max 15 W power; • Laser generator beam: Gaussian-Like beam; • The beam is shaped by line pattern diffusion lens;
Laser-line scanning	• Incidence angle to samples surface: 50°; • Scanning speed: 20 mm/s;
Image sampling of IR camera	• 25 Hz sampling rate; 20 s sampling duration; • 500 images captured for each experiment;

results demonstrate the feasibility of the proposed approach for the impact damage combined with multiple defect portions. It sets a solid foundation for applicability testing on real impact damage samples in the next stage.

4.2. Experimental setup system

To validate the proposed damage detection and visualisation technique experimentally, a laser-line scanning thermography testing system was established for the inspection of combined damage in the CFRP samples shown in Fig. 1. The full view of the testing system is shown in Fig. 7. The CFRP samples were heated by a scanning laser-line beam controlled by an X-Y translation stage. The thermal images were captured by a FLIR-A615 series long-wave (7–14 μm) IR camera. Table 2 gives the key technical specifications of the camera and the laser excitation source associated with the detailed experimental parameters. Between each experiment, a 10-minute interval was applied to cool the specimen.

Fig. 8 shows the double sides of five impact damage CFRP samples subjected to different impact energies from 10 J to 30 J. The specimens were produced with a standard drop test. The specification of specimens and drop testing are stated in Table 3. The strike dents and damage with unpredictable directions are mixed and clearly visible from the impacted side. But on the rear surface, the damage appearing as a form of combined damage with delamination overlapping with cracks are hidden or less obvious. All the rear sides of five CFRP samples were tested using the above experimental system. Considering different testing environments, three laser scanning modes: parallel, 45°

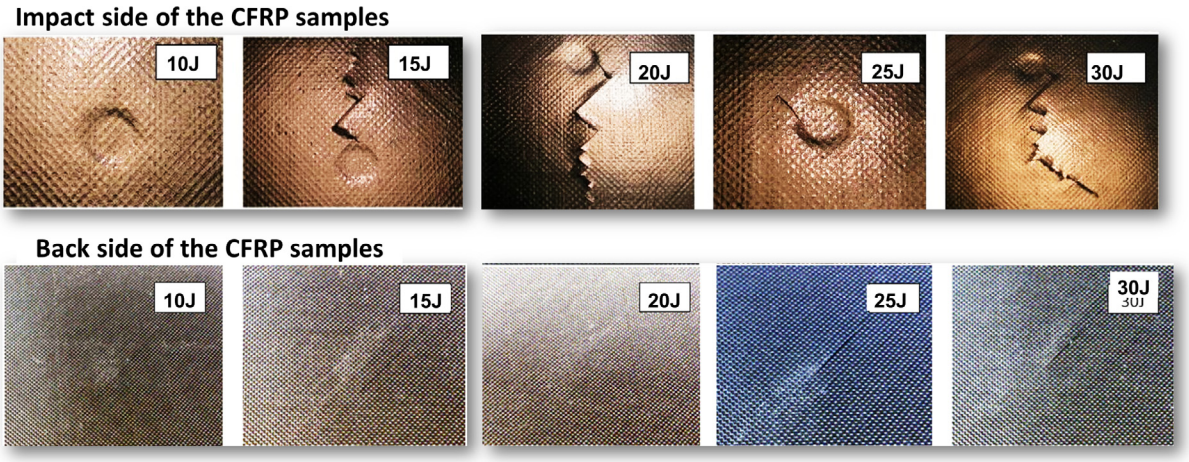

Fig. 8. Snapshots of five studied impacted CFRP specimens; (a) Impact damage is visible from the impacted side; (b) The rear surface of the samples presented invisible or unobvious evidence of combined damage (mainly composed by matrix cracks and delamination).

Table 3
Composite samples and corresponding impact testing specifications.

Items	Sample Information
Composite dimensions	• Amount: 5 • 150 mm × 100 mm × 4 mm
Material	• Hexply pre-impregnated M21/35%/198/T800 plies comprising of plys with thickness around 180–200 μm. • unidirectional Toray 800 carbon fibres; • Hexcel M21 epoxy resin; • Quasi-isotropic and symmetric configuration (stacking sequence)
Impact testing	• Drop impact test with predefined energy levels using a semi-spherical 16 mm diameter weight drop machine; • Drop weight of 2.281 kg; • Gravitational acceleration: 9.8 m/s^2 • Standard used: BS ISO 18352;
Impact damage	• Drop height (m): 0.45, 0.67, 0.89, 1.12. 1.34; • Energy (J): 10, 15, 20, 25, 30;

and orthogonal inspection modes (intersection angle between fibre direction and laser-line) were tested.

4.3. Experimental results

To implement the proposed method, the spatial (each combined defect area) and transient Region Of Interest (ROI) image sequence (images sub-set of laser scanning across the whole defect) was extracted. The data captured using the parallel inspection mode for the 30 J defect sample (biggest defect) were initially discussed.

Fig. 9 presents a raw temperature image when the laser-line is right on the crack and its 4-level SWT decomposition coefficients using the 'Haar' wavelet basis. It is observed that the different image properties (noise, crack, delamination) are separately enhanced by different levels of the coefficient. Focusing on each level, the coefficients in level-1 and level-2 mainly present the high-frequency noises and crack

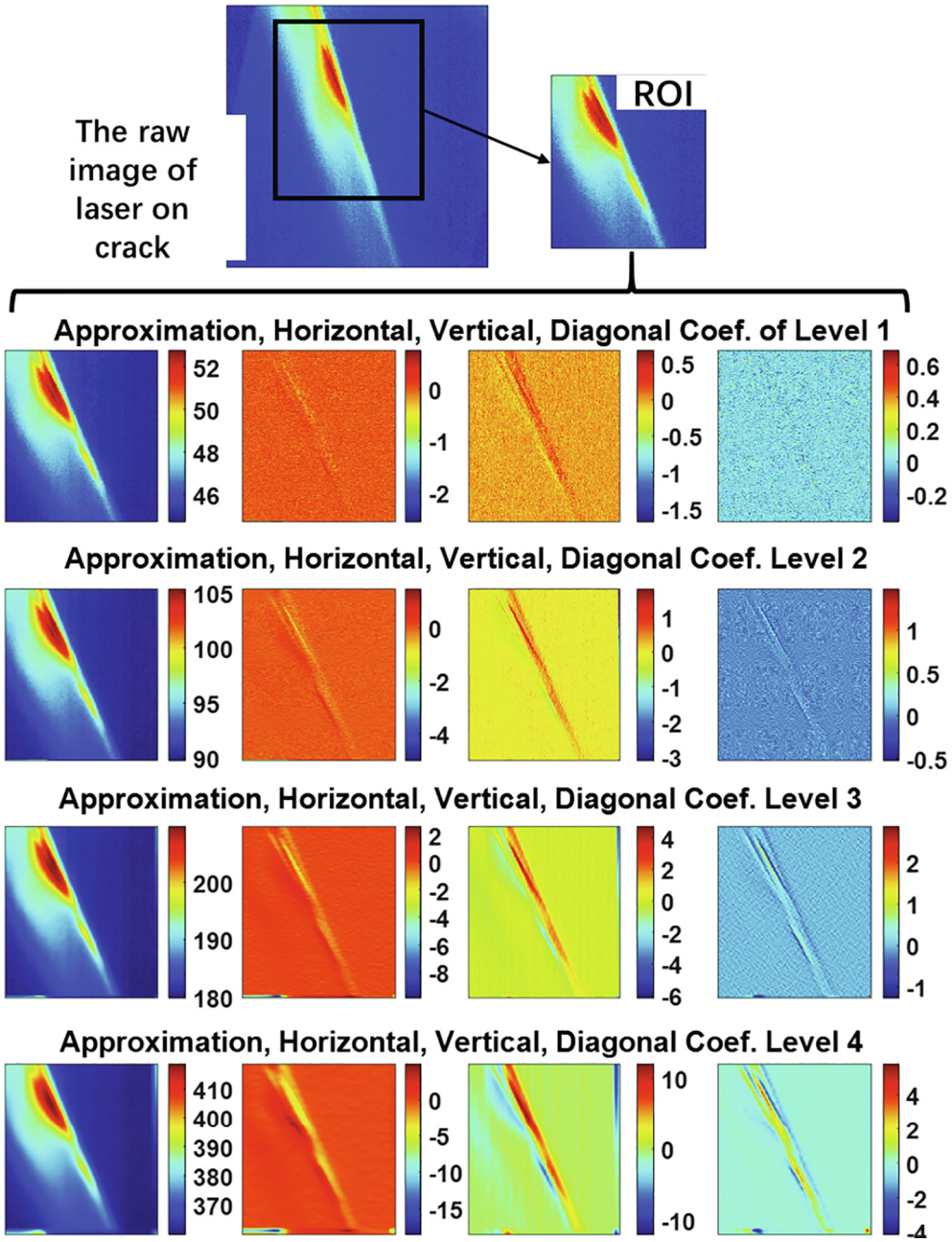

Fig. 9. The coefficients of SWT decomposition of a thermal image.

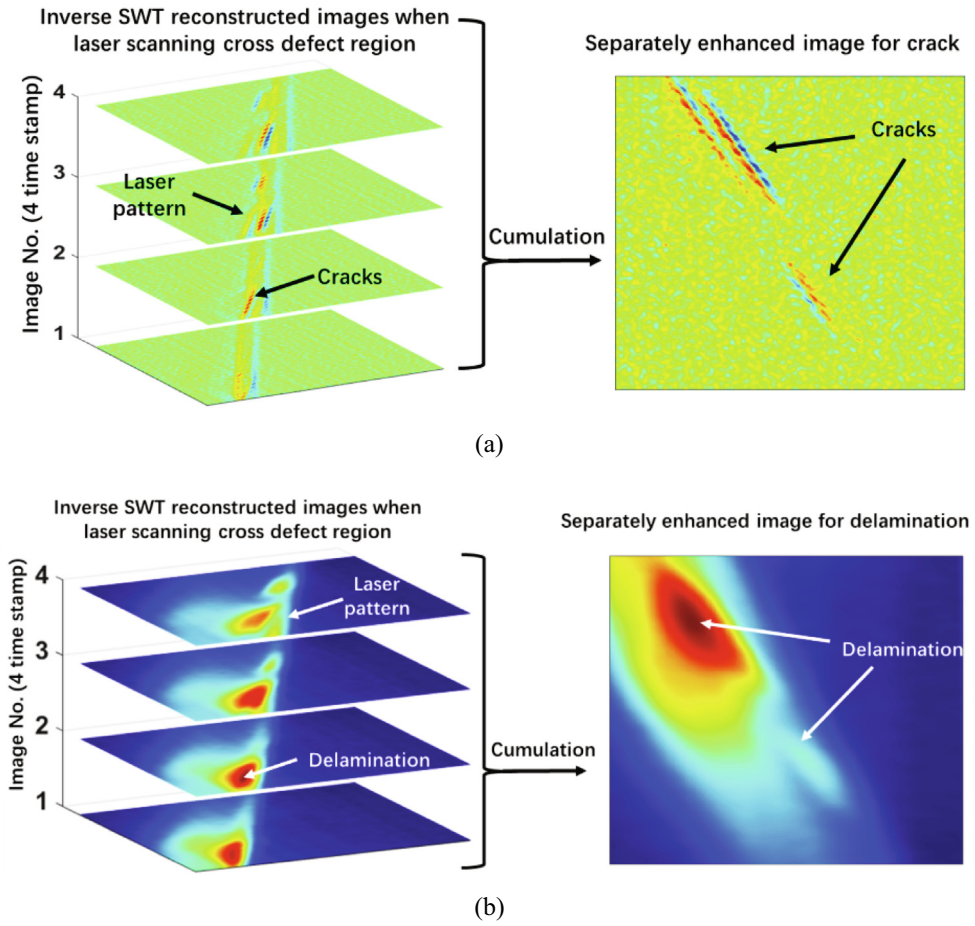

Fig. 10. The Inverse SWT reconstructed results and cumulation results for cracks and delamination results. (a) Crack targeted enhancement; (b) Delamination targeted enhancement;

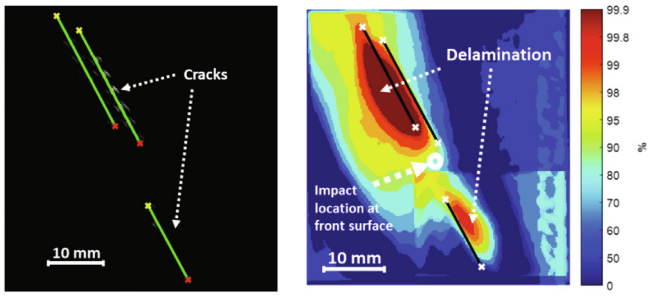

Fig. 11. Defect calibration of combined defects of 30 J samples; (a) Cracks extraction by RANSAC; (b) Fusion image of cracks and delamination confidence map;

properties, respectively. The coefficients in level-3 contain the laser-line pattern and a part of crack properties, while level-4 coefficients represent most of the low-frequency delamination properties with smooth spatial variation.

As shown in the proposed methodology, the level-4 coefficients will be preserved while other levels will be eliminated (set to 0) for delamination enhancement. For cracks, we found that the level-3 coefficients have stronger contrast on crack than the level-2 coefficients even though the laser-line edges are also be captured. The level-3 coefficients will be preserved for cracks enhancement and the image sequence cumulation strategy is used to eliminate the laser pattern.

By selecting level-3, level-4 wavelet coefficients for crack and delamination enhancement respectively, the reconstructed images of ROI for crack and delamination are shown in Fig. 10(a) and (b) respectively. In the left stacked images of Fig. 10(a) and (b), four temporal reconstructed images of laser scanning over on defects are presented, and the high-frequency noise is remarkably reduced. The inverse SWT reconstructed images effectively enhance the crack and delamination features using corresponding frequency properties, respectively, although few dynamic laser patterns are still there. By using the cumulation strategy, the dynamic laser patterns are considerably eliminated, and the still defect feature is further enhanced (see the right part of Fig. 10(a) and (b)). These results demonstrate that the method based on the selection of wavelet frequency properties has good performance on the enhancement of different defect feature and noise cancellation. The combination of cumulation strategy eliminates the laser heating pattern which is hard to separate to crack feature in the wavelet domain. The proposed wavelet-based methodology effectively deals with disturbance of noise, laser pattern, and returns with a clean and high contrast visualisation for different defect properties.

In the enhanced images of crack and delamination, two combined damage regions (two cracks regions paired with two delamination regions) can be observed in Fig. 10, and there is no overlapping between two defect regions. Therefore, it is rational to separately focus on each ROI for each crack extraction and delamination calibration by the confidence map.

Fig. 11(a) shows the extracted three cracks (marked with green lines) from combined damage by the RANSAC algorithm. Based on

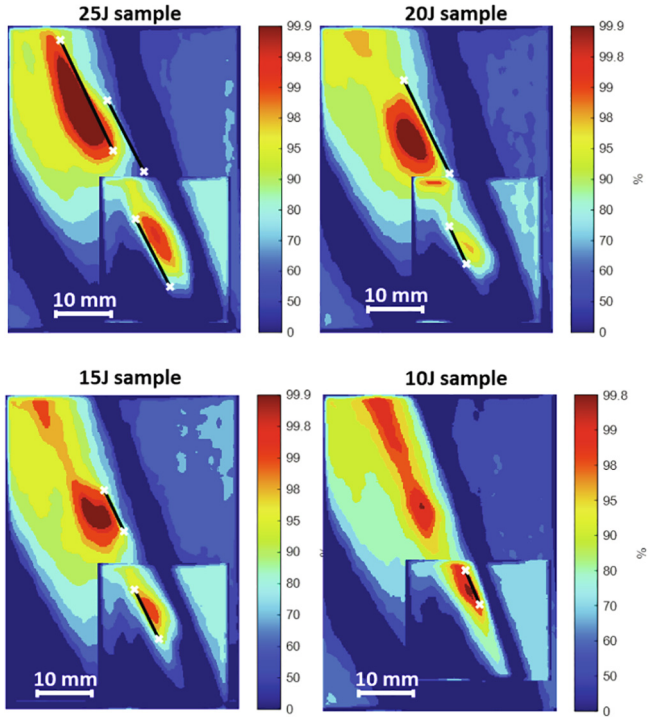

Fig. 12. Defect calibration of combined defects of parallel inspection model (laser-line parallel with fiber direction) of 4 samples (25 J, 20 J, 15 J and 10 J impact samples);

the enhanced crack feature image, the RANSAC algorithm presents effective straight lines extraction. Fig. 11(b) shows the fused confidence map profile for two delaminations and also with crack lines in combined damage. In the confidence map, the delamination position and shape are represented by the contour map profile. The confidence map level provides an indicator representing the delaminated degree of samples which is an effective foundation for actual delamination defect boundary extraction.

Based on the proposed method, the defect results of the other 4 samples (samples with 25 J, 20 J, 15 J and 10 J impact) are shown in Fig. 12. The lower impact energy induced, the smaller combined damage are generated at both surfaces. As expected, the crack length and delamination area decrease with the impact energy. In the 30 J and 25 J samples, the upper combined damage has two obvious surface open cracks while others have only one or no crack. The fusion images also show that all samples have two impact combined damage areas. Two delamination and cracks have similar form and are separately distributed at the two sides of the impact location (front surface). The results show that the impact may cause double combined damage region at both surfaced. The form of one combined damage contains crack distributed at one side of the delamination. In addition, the smaller the combined damage is, the defect shape contrast is more influenced by the laser-line pattern.

Considering the actual diversity of scanning condition, the defect results from the 45°intersection angle and orthogonal scanning modes are presented in Figs. 13 and 14 respectively. The first image gives the scanning mode distribution by one of the raw thermal images, and the defect visualisation results in terms of confidence map for both crack and delamination are listed. The two combined damage in each sample can be clearly detected in these visualisation results. It demonstrates

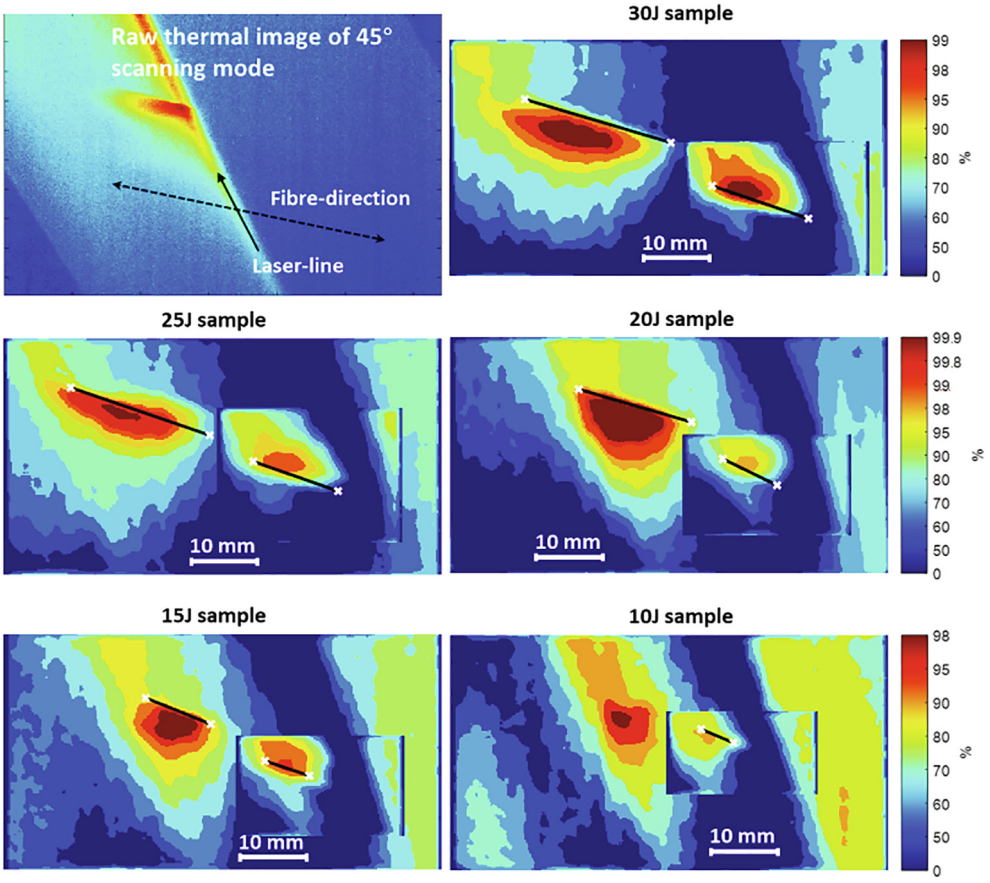

Fig. 13. Defect calibration of combined defects of 45° scanning mode (laser-line 45° with fiber direction) of 5 samples (30 J, 25 J, 20 J, 15 J and 10 J impact samples);

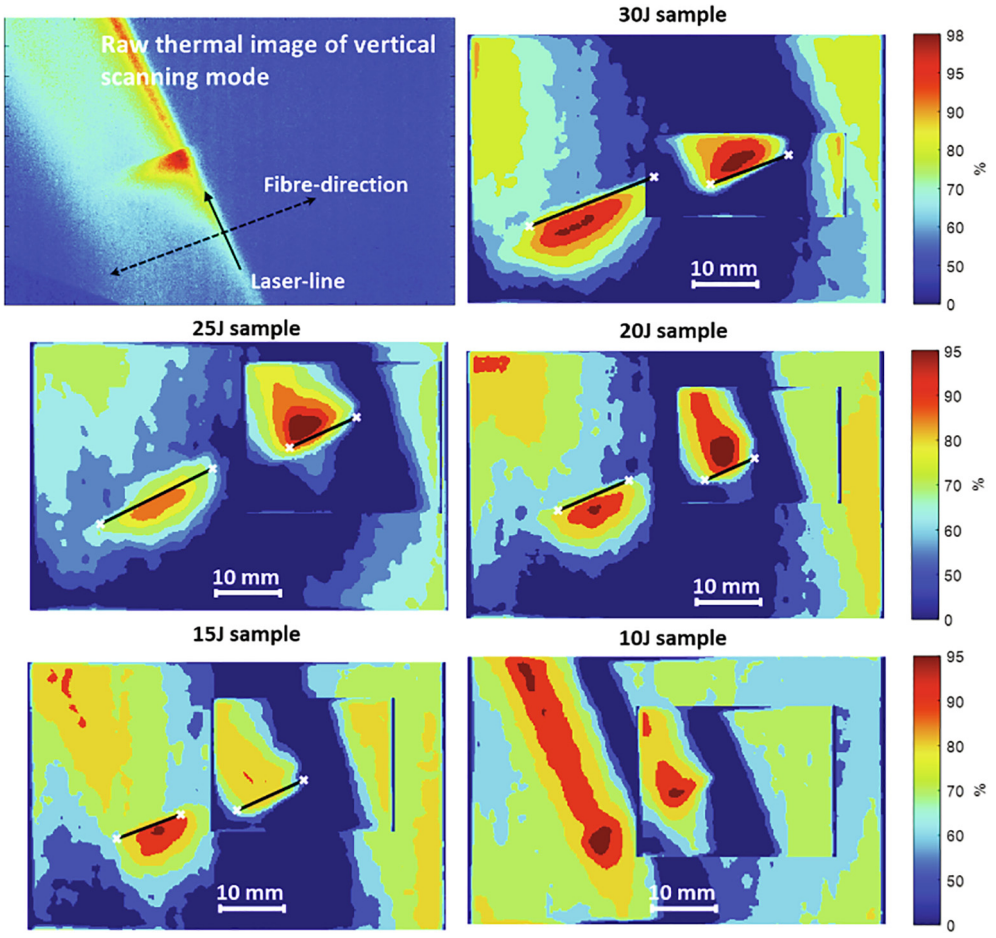

Fig. 14. Defect calibration of combined defects of vertical scanning mode (laser-line perpendicular to fibre direction) of 5 samples (30 J, 25 J, 20 J, 15 J and 10 J impact samples);

that the proposed methodology has wide applicability to different scanning and defect directions. However, it is admittedly that different scanning modes have various sensibility on inspected defect contrast and dimension. From the visualised results, for the 30 J and 25 J samples, the 45°and orthogonal scanning mode can only detect two cracks while there are three cracks detected in the parallel mode. Similarly, for each delamination, the smallest delamination area indicated by confidence contour profile can be found in the orthogonal scanning mode. In contrast, the parallel mode produced a bigger defective area than the other two modes. In this research, damages in all investigated samples have the structure which the delamination concentrates at one side (left or right) of the crack. But the proposed method is effective to consider the symmetry of the damage on both sides of the crack, as long as the captured thermal images exhibit such features.

It should be noted that multiple wavelets basis have been attempted to test the performance variantion including “Haar”, “Mexh”, “Morlet”, “Symlet” family, “Coif” family, and “db” family. It was found that “Haar” can achieve a better balance for the enhancement of crack edge and delamination profile in one process in this research. However, the proposed approach is an open method which the optimal wavelet basis may vary in applications with different materials and defects structure.

5. Conclusion

Low-velocity impact-induced combined damage is one of the most typical but challenging structural degradations in CFRP laminates, commonly composed of in-plane (i.e. in-ply) transverse crack and inter-laminar delamination damage properties prior to fibre breakage. The underlying physical law of damage propagation for single-type damage would not be reliably appliable to advanced laminates at structursal scale. Prior to the realization of the true effect of such complex damages, each type of damage must be characterised separately. To pertinently inspect and analyse each main portion in the combined damage, this article proposes a dissection, enhancement and characterisation technique for the inspection of individual BVIDs in composite laminates using the laser-line scanning thermography. Firstly, a FEM model representing multi-layered unidirectional CFRPs with existing combined matrix crack and inter-laminar delamination is proposed to predict the thermal image feature of the damage in laser scanning inspection. The simulated thermal pattern shows diverse but overlapped and interfering defect feature corresponding to the crack and delamination. Secondly, a SWT-based damage feature decomposition and enhancement strategy for thermal image sequence is proposed to extract the crack and delamination driven thermal properties for contrast improvement, meanwhile ordinating noise elimination and laser background suppression. Based on the enhanced defect feature, the RANSAC and confidence map algorithms are applied to furtherly analyse the crack and delamination with quantifiable crack lines and confidence contour profile. Finally, the enhanced results of three scanning inspection modes demonstrate the remarkable flexibility of the proposed method with multiple BVID samples. The research pushes a solid step for impact combined damage inspection and damage properties quantification, remarkably progressing in automated IR image sequence data processing for composite laminates.

It should be noted that the proposed method focuses on the separation and contrast enhancement of the two main crack and delamination in impact combined damage at the same time. The applicability of this method for tiny fibre break damage will require further study. More future investigation will be implemented on the quantification reconstruction and dissection of penetration level and depth of the crack and delamination in the combined damage. In addition, the selection of the wavelet basis was based on the parallel scan mode, the study of optimal wavelet selection according to scanning diversity will be investigated in the following research.

CRediT authorship contribution statement

Haochen Liu: Conceptualization, Methodology, Validation, Formal analysis, Investigation, Data curation, Writing - original draft. **Weixiang Du:** Investigation, Data curation. **Yazdani Nezhad Hamed:** Validation, Writing - review & editing. **Andrew Starr:** Resources, Writing - review & editing. **Yifan Zhao:** Conceptualization, Methodology, Validation, Formal analysis, Writing - original draft.

Declaration of Competing Interest

The authors declare that they have no known competing financial interests or personal relationships that could have appeared to influence the work reported in this paper.

Acknowledgement

The data that support the findings of this study are openly available in the Cranfield University repository, CORD, at DOI: http://doi.org/10.17862/cranfield.rd.14668968.

References

[1] Irving P, Soutis C. Polymer composites in the aerospace industry. Cambridge, UK: Woodhead Pub; 2015.
[2] Hernandez TPA, Mills AR, Yazdani Nezhad H. Shear driven deformation and damage mechanisms in high-performance carbon fibre-reinforced thermoplastic and toughened thermoset composites subjected to high strain loading. Compos Struct 2021;261:113289. https://doi.org/10.1016/j.compstruct.2020.113289.
[3] Yuan S, Ren Y, Qiu L, Mei H. A multi-response-based wireless impact monitoring network for aircraft composite structures. IEEE Trans Indus Electron 2016;63(12):7712–22.
[4] V. Kumar, T. Yokozeki, C. Karch, et.al., "Factors affecting direct lightning strike damage to fiber reinforced composites: A review", Compos B Eng vol. 183, 2020.
[5] Yazdani Nezhad H, Zhao Y, Liddel PD, Marchante V, Roy R. A novel process-linked assembly failure model for adhesively bonded composite structures. CIRP Ann 2017;66(1):29–32.
[6] Nezhad HY, Stratakis D, Ayre D, Addepalli S, Zhao Y. Mechanical performance of composite bonded joints in the presence of localised process-induced zero-thickness defects. Procedia Manuf 2018;16:91–8.
[7] González EV, Maimí P, Camanho PP, Turon A, Mayugo JA. Simulation of drop-weight impact and compression after impact tests on composite laminates. Compos Struct 2012;94(11):3364–78.
[8] Nezhad HY, Merwick F, Frizzell RM, McCarthy CT. Numerical analysis of low-velocity rigid-body impact response of composite panels. Int J Crashworthiness 2015;20(1):27–43.
[9] M. Fikry, R. Kitamura, S. Ogihara, Effect of matrix cracking on mechanical properties in FRP angle-ply laminates, P Mat Mech Conf, vol. 2017, no. 0, p. OS1014, 2017.
[10] Wisnom MR. The role of delamination in failure of fibre-reinforced composites. Phil Trans R Soc A 2012;370(1965):1850–70.
[11] Liu Y, Liu K, Yang J, Yao Y. Spatial-neighborhood manifold learning for nondestructive testing of defects in polymer composites. IEEE Trans Industr Inform 2020;16(7):4639–49.
[12] Riccio A, Saputo S, Sellitto A, Di Caprio F. On the crashworthiness behaviour of a composite fuselage Sub-floor component. Compos Struct 2020;234:111662.
[13] Sadighi M, Alderliesten RC, Benedictus R. Impact resistance of fiber-metal laminates: A review. Int J Impact Eng 2012;49:77–90.
[14] B. Wang, S. Zhong, T. Lee, KS. Fancey,J. Mi. "Non-destructive testing and evaluation of composite materials/structures: A state-of-the-art review". Adv Mech Eng, vol. 12, no. 4, 2020.
[15] Zhao Y, Tinsley L, Addepalli S, Mehnen J, Roy R. A coefficient clustering analysis for damage assessment of composites based on pulsed thermographic inspection. NDT E Int 2016;83:59–67.
[16] Sirikham A, Zhao Y, Nezhad HY, Du W, Roy R. Estimation of damage thickness in fiber-reinforced composites using pulsed thermography. IEEE Trans Industr Inform 2019;15(1):445–53.
[17] Comer AJ, Katnam KB, Stanley WF, Young TM. Characterising the behaviour of composite single lap bonded joints using digital image correlation. Int J Adhesion Adhes 2013;40:215–23.
[18] Maierhofer C, Röllig M, Ehrig K, Meinel D, Céspedes-Gonzales G. Validation of flash thermography using computed tomography for characterizing inhomogeneities and defects in CFRP structures. Compos Part B Eng 2014;64:175–86.
[19] Gaudenzi P, Bernabei M, Dati E, De Angelis G, Marrone M, Lampani L. On the evaluation of impact damage on composite materials by comparing different NDI techniques. Compos Struct 2014;118:257–66.
[20] Sellitto A, Riccio A, Russo A, Zarrelli M, Toscano C, Lopresto V. Compressive behaviour of a damaged omega stiffened panel: Damage detection and numerical analysis. Compos Struct 2019;209:300–16.
[21] Shi Q, Liu J, Liu W, Wang F, Wang Y. Barker-coded modulation laser thermography for CFRP laminates delamination detection. Infrared Phys Technol 2019;98:55–61.
[22] Hwang S, An Y-K, Kim J-M, Sohn H. Monitoring and instantaneous evaluation of fatigue crack using integrated passive and active laser thermography. Optics Lasers Eng 2019;119:9–17.
[23] Moran J, Rajic N. "Remote line scan thermography for the rapid inspection of composite impact damage," (in English). Compos Struct 2019;208:442–53.
[24] Qiu J, Pei C, Liu H, Chen Z, Demachi K. Remote inspection of surface cracks in metallic structures with fiber-guided laser array spots thermography. NDT E Int 2017;92:213–20.
[25] J.C. Wei, F. Wang, J.Y. Liu, Y. Wang, L. He, A laser arrays scan thermography (LAsST) for the rapid inspection of CFRP composite with subsurface defects, Compos Struct 2019;226.
[26] A.I. Moskovchenko, V.P. Vavilov, R. Bernegger, "Detecting delaminations in semitransparent glass fiber composite by using pulsed infrared thermography". J Nondestr Eval, vol. 39, no. 69, 2020.
[27] Liu H, Pei C, Xie S, Li Y, Zhao Y, Chen Z. Inversion technique for quantitative infrared thermography evaluation of delamination defects in multilayered structures. IEEE Trans Industr Inform 2020;16(7):4592–602.
[28] He Y, Tian G, Pan M, Chen D. Impact evaluation in carbon fiber reinforced plastic (CFRP) laminates using eddy current pulsed thermography. Compos Struct 2014;109:1–7.
[29] Liang T, Ren W, Tian GY, Elradi M, Gao Y. Low energy impact damage detection in CFRP using eddy current pulsed thermography. Compos Struct 2016;143:352–61.
[30] Shi Y, Swait T, Soutis C. Modelling damage evolution in composite laminates subjected to low velocity impact. Compos Struct 2012;94(9):2902–13.
[31] Riccio A, Caputo F, Di Felice G, Saputo S, Toscano C, Lopresto V. A joint numerical-experimental study on impact induced intra-laminar and inter-laminar damage in laminated composites. Appl Compos Mater 2016;23(3):219–37.
[32] Lopez F, de Paulo Nicolau V, Ibarra-Castanedo C, Maldague X. Thermal–numerical model and computational simulation of pulsed thermography inspection of carbon fiber-reinforced composites. Int J Therm Sci 2014;86:325–40.
[33] Wang J, Carson J, North M, Cleland D. A new approach to modelling the effective thermal conductivity of heterogeneous materials. Int J Heat Mass Transfer 2006;49(17–18):3075–83.
[34] Solbo S, Eltoft T. A stationary wavelet-domain wiener filter for correlated speckle. IEEE Trans Geosci Remote Sensing 2008;46(4):1219–30.
[35] Liu T, Zhang W, Yan S. A novel image enhancement algorithm based on stationary wavelet transform for infrared thermography to the de-bonding defect in solid rocket motors. Mech Syst Signal Process 2015;62-63:366–80.
[36] Hast A, Nysjö J, Marchetti A. Optimal RANSAC – Towards a Repeatable Algorithm for Finding the Optimal Set (PDF). J WSCG 2013;21(1):21–30.
[37] Zhao Y, Addepalli S, Sirikham A, Roy R. A confidence map based damage assessment approach using pulsed thermographic inspection. NDT E Int 2018;93:86–97.